ADVANCED FUNCTIONAL MATERIALS
www.afm-journal.de

Materials Views
www.MaterialsViews.com

Epitaxial Growth of PbSe Quantum Dots on MoS_2 Nanosheets and their Near-Infrared Photoresponse

Julia Schornbaum, Benjamin Winter, Stefan P. Schießl, Florentina Gannott, Georgios Katsukis, Dirk M. Guldi, Erdmann Spiecker, and Jana Zaumseil**

A facile one-pot synthesis of hybrid materials consisting of PbSe quantum dots (QDs) that grow epitaxially on MoS_2 nanoflakes resulting in three equivalent orientation variants of the PbSe QDs with respect to the MoS_2 lattice is demonstrated. The epitaxial growth and cross-sectional high-resolution transmission electron microscopy (HRTEM) investigations verify a direct and linker-free contact between the quantum dots and the transition metal dichalcogenide (TMD) nanoflakes, while maintaining surface passivation of the PbSe with oleic acid ligands on the outside. Solution-processed photodetectors based on PbSe-MoS_2 hybrids exhibit stable photoconduction when illuminated with near-IR light (wavelength > 1200 nm) without any laborious ligand-exchange steps. Flexible devices fabricated on polyethylene terephthalate (PET) substrates show excellent stability upon repeated bending. These hybrid materials are air-stable and solution-processable at low temperatures and thus promising for low-cost flexible near-IR photodetectors.

1. Introduction

Transition metal dichalcogenides (TMDs) are a well-known class of layered materials whose properties range from semiconducting to metallic and superconducting.[1] In recent years renewed interest in these materials has developed due to the unique optical and electronic properties of their monolayers and hence potential for novel applications in optoelectronics.[2–10] In TMDs such as MoS_2 and WS_2, each layer is composed of three covalently bonded atomic sheets, for example, S–Mo–S in MoS_2. The individual layers are held together only by van-der-Waals forces and thus multi- or monolayer flakes can be obtained by mechanical exfoliation or ultrasonication.[3–5,11,12] In its bulk form, MoS_2 is a semiconductor with an indirect band gap of 1.2 eV (≈1030 nm). The band gap of a monolayer of MoS_2 is direct and increases to 1.8 eV (≈690 nm).[6,7,10] Monolayer MoS_2 also shows good electron mobilities (up to 200 $cm^2\ V^{-1}\ s^{-1}$).[6] High carrier mobilities, large surface area, and solution processability make MoS_2 nanomaterials interesting for application in photodetectors that rely on fast charge separation and transport.[8,13,14] Hybrids with semiconductor quantum dots (QDs) would allow for extending and fine-tuning the spectral response in the near-infrared.

Semiconductor QDs with their size-tunable absorption are ideal building blocks for nanohybrid materials and have been used as light-absorbing materials in various photodetectors and photovoltaic devices.[15–24] However, the charge transport in QD-based optoelectronic devices is challenging. The large number of grain boundaries in thin films of QDs increase the probability of electron-hole recombination before charges are extracted at the electrodes.[25] The possibility to enhance charge separation and transport by the formation of nanohybrids of QDs and high mobility materials in order to obtain highly sensitive photoconductive devices has been recognized and pursued.[26–28] TMDs seem perfect for such nanohybrids. Thin flakes of MoS_2 (monolayers or multilayers) could be expected to act as a semiconducting support for QDs and to facilitate the transformation of the photoexcited states of the light-harvesting QDs into charge-separated states. Moreover, fewer grain boundaries and faster charge transport in MoS_2 flakes than in conventional thin QD films should boost the photosensitivity and shorten response times. This concept was applied successfully with QD-graphene hybrids as active layers in photodetectors[28–35] but no hybrid materials of semiconducting QDs and any of the other layered materials have been used until now. In addition, processing conditions and air-stability are important concerns for hybrid photodetectors. Wet-chemical processes forming low-cost solution-processable, air-stable hybrids, without any laborious ligand exchange would be highly advantageous.

We chose PbSe-MoS_2 as a hybrid material for the fabrication of photodetectors. This particular material combination

J. Schornbaum, S. P. Schießl, F. Gannott, Prof. J. Zaumseil
Department of Materials Science
Nanomaterials for Optoelectronics Group
Friedrich-Alexander-Universität Erlangen-Nürnberg
91058, Erlangen, Germany
E-mail: jana.zaumseil@fau.de

B. Winter, Prof. E. Spiecker
Department of Materials Science
Center for Nanoanalysis and Electron Microscopy
Friedrich-Alexander-Universität Erlangen-Nürnberg
91058, Erlangen, Germany
E-mail: erdmann.spiecker@ww.uni-erlangen.de

G. Katsukis, Prof. D. M. Guldi
Department of Chemistry and Pharmacy
Chair of Physical Chemistry I
Friedrich-Alexander-Universität Erlangen-Nürnberg
91058, Erlangen, Germany

DOI: 10.1002/adfm.201400330

is promising with regard to the demand of a direct contact between the two materials. Indeed, atomically sharp interfaces between cubic (rock-salt) monochalcogenides MX (M = Pb, Sn, Sb, Bi, or rare earth metal; X = S, Se, or Te) and layered dichalcogenides TX_2 (T = early transition metal) are well known as part of the large class of misfit-layered compounds $[(MX)_{1+\delta}]_m[TX_2]_n$ that consist of alternatingly stacked layers of the two materials.[36,37] Such interfaces show an epitaxial relationship even though the two crystal lattices do not match in symmetry resulting in large unit cells or even incommensurate structures.[37–39] The misfit-layered compounds can also be viewed as intercalation compounds with TX_2 representing the host crystal and MX as the intercalate. The intercalation leads to new properties such as a change in the electronic features of the host structure due to charge transfer from the MX part to the TX_2 layer.[40,41]

Based on the epitaxial arrangement of mono- and dichalcogenides in misfit-layered compounds, an epitaxial growth of the PbSe QDs on MoS_2 is expected under sufficiently clean conditions. Epitaxial growth is advantageous as it results in a defined and direct interface between PbSe QDs and MoS_2, without any linker molecule in between. A direct interface is important for the application of PbSe-MoS_2 hybrids in photodetectors to achieve charge transfer from the PbSe QDs to the MoS_2. Usually epitaxial growth of nanoparticles (e.g., Pt) on crystalline inorganic materials (e.g., $SrTiO_3$) is accomplished by vapor-phase deposition methods.[42,43] These physical methods are more complex than wet-chemical methods, less scalable and often require ultra-high vacuum conditions and specialized equipment. Therefore, it is sensible to explore an in situ wet-chemical synthesis to combine PbSe QDs and MoS_2 nanoflakes directly. A wet-chemical synthesis is also advantageous in terms of solution processability of the resulting PbSe-MoS_2 hybrid materials. Polymer foils, e.g., polyethylene terephthalate (PET) or polyimide (PI), are suitable substrates for flexible electronics including detectors, displays, and sensors. They are durable and lightweight but cannot withstand high temperatures (>150 °C). Traditional photodetector materials, e.g., bulk PbS or Si, are processed using high-temperature manufacturing techniques. Consequently, these photodetectors cannot be fabricated on polymer substrates. In contrast, low-temperature solution processable PbSe-MoS_2 hybrids should be applicable for fabrication on flexible plastic substrates such as PET.[44,45]

Here, we introduce a simple one-pot synthesis for PbSe QD-MoS_2 hybrids, which is also applicable to few-layer graphene (FLG) and WS_2 multilayered nanoflakes. This in situ synthesis leads to a direct epitaxial growth of PbSe QDs on MoS_2. No further ligand exchange steps are required. We demonstrate the near-infrared photosensitivity of these PbSe-MoS_2 hybrids, which are solution-processable at low temperatures and long-term air-stable. The new PbSe-MoS_2 hybrid material also shows excellent mechanical stability on a PET substrate upon repeated bending.

2. Results and Discussion

Figure 1a,b show representative transmission electron microscopy (TEM) images of PbSe-MoS_2 hybrids. The PbSe QDs were

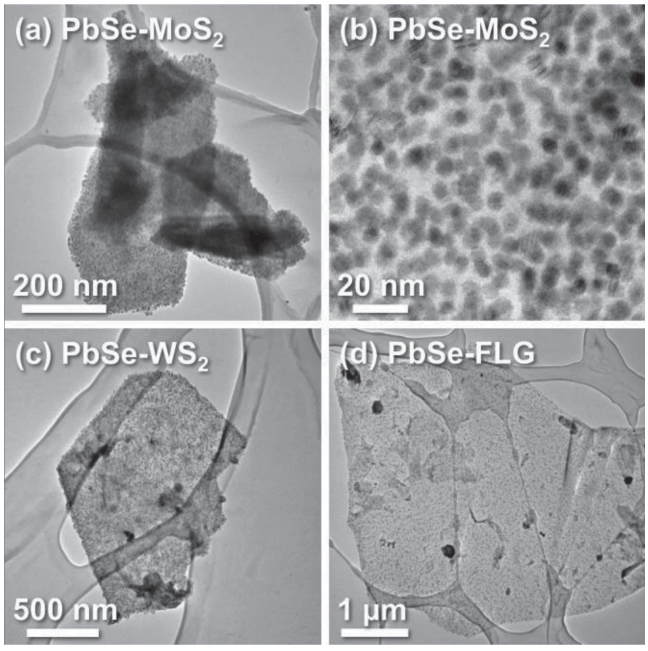

Figure 1. TEM images of hybrid materials of a) PbSe-MoS_2, c) PbSe-WS_2, d) PbSe-FLG. b) HRTEM image of the PbSe-MoS_2 hybrid material showing the average size of 5.7 nm of the PbSe QDs, corresponding to a band gap of 0.74 eV; absorption edge 1675 nm.

synthesized in presence of exfoliated MoS_2 nanoflakes. For this one-pot synthesis we used a standard air-free Schlenk-line technique and the hot-injection method. Briefly, Pb(oleate)$_2$ was formed by mixing PbO, oleic acid, and 1-octadecene. At the same time, dispersions of MoS_2 nanoflakes were produced by ultrasonication of MoS_2 powder in diphenyl ether and subsequent centrifugation. The Raman spectrum of exfoliated MoS_2 with PbSe QDs (PbSe itself shows no Raman signals) was similar to that of bulk MoS_2 and thus indicating mostly multilayered flakes (see Figure S1, Supporting Information). This was also supported by the contrast in conventional TEM images (Figure S2, Supporting Information) and, more directly, by cross-sectional high-resolution (HR) TEM (vide infra) and convergent beam electron diffraction (CBED) (Figure S3, Supporting Information), both indicating typical flake thicknesses of a few tens of nanometers. In a subsequent step, the MoS_2 dispersion was injected into the solution of Pb(oleate)$_2$. In order to start the PbSe QD growth, selenium dissolved in tri-*n*-octylphosphine was injected into the Pb(oleate)$_2$-MoS_2 solution at 170 °C. PbSe-MoS_2 hybrids were formed within 5 min. We used Pb^{2+} and Se^{2-} in large excess compared to the concentration of the MoS_2 flakes in order to obtain full and dense coverage of the flakes with PbSe QDs. As a consequence, PbSe QDs not only grew on the flakes but also in solution. The PbSe-MoS_2 hybrids were easily separated from any unbound PbSe QDs by centrifugation. They precipitated from hexane whereas the unbound QDs remained in dispersion. The representative TEM image in Figure 1a was taken after the separation process and confirmed the absence of any free QDs in the hybrid samples. Energy-dispersive X-ray spectroscopy (EDX) corroborated the expected composition of the hybrid (Figure S4, Supporting Information). In order to test the general applicability

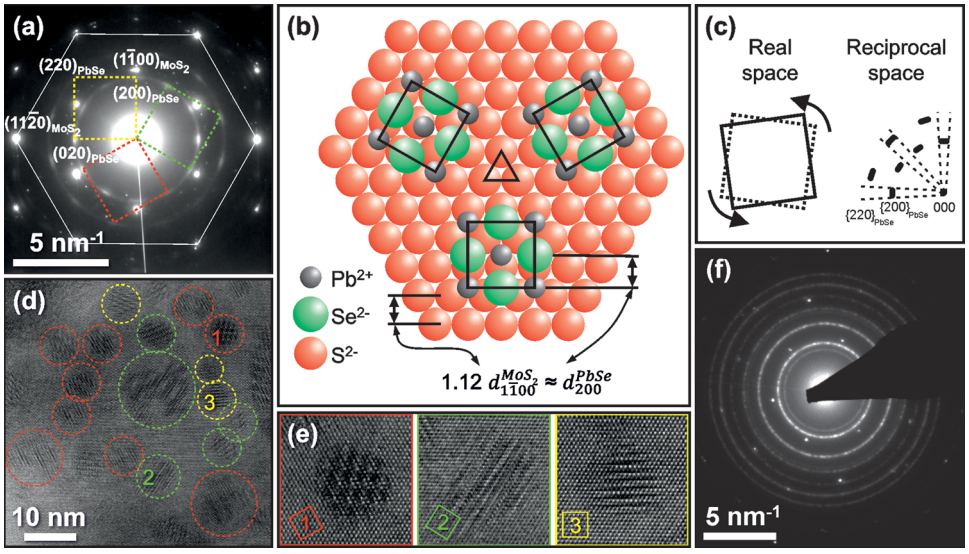

Figure 2. a) SAED pattern of the in situ synthesized PbSe-MoS_2 hybrid material revealing a preferred orientation of PbSe QDs on the MoS_2 nanoflake, represented by the red, green, and yellow squares, whereas the white hexagon indicates the hexagonal arrangement of MoS_2. b) Schematic illustration of the epitaxial relationship between the PbSe QDs and MoS_2 flakes, showing the three equivalent orientation variants of the PbSe QDs and c) schematic illustration of the elongation of the diffraction points in reciprocal space (diffraction pattern) by rotation of the PbSe unit cell in real space. d) HRTEM image of the PbSe-MoS_2 hybrid showing the three orientation variants marked in red, green and yellow and e) enlarged HRTEM images of the QDs at positions 1, 2, and 3 of panel (d). f) SAED pattern of separately synthesized PbSe QDs mixed, upon heating to 170 °C for 4 h under inert gas, with exfoliated MoS_2 showing no preferential orientation of the PbSe QDs on the MoS_2 nanoflake.

of the developed synthesis we also used WS_2 multilayer sheets and FLG, instead of MoS_2, to grow PbSe QDs in situ on these materials. The TEM images in Figure 1c,d clearly show PbSe QDs on WS_2 and FLG confirming the general feasibility of this procedure for growing PbSe QDs on a wide range of layered materials.

The bond between the PbSe QDs and MoS_2 nanoflakes was quite strong. Even upon repeated washing and ultrasonication cycles the particles could not be removed from the flakes. Therefore, detailed selected-area electron diffraction (SAED) and HRTEM investigations were performed to elucidate the growth mechanism of the PbSe QDs and the interface between the QDs and the MoS_2 nanoflakes. The SAED pattern of the hybrid material in **Figure 2**a shows PbSe reflections (rock-salt structure) in addition to the characteristic hexagonal arrangement of MoS_2 reflections expected for electron illumination along $<0001>^{MoS_2}$, i.e., perpendicular to the basal plane. The diffraction pattern of the QDs reveals distinct ring fragments on the $\{200\}_{PbSe}$ and $\{220\}_{PbSe}$ diffraction rings rather than continuous rings with constant intensity. Moreover, diffraction rings of type $\{111\}_{PbSe}$ and $\{311\}_{PbSe}$ are completely absent. Taken together these observations point to a $<001>_{PbSe}$ growth direction of the PbSe QDs on the MoS_2 nanoflakes and a preferred in-plane orientation indicative of epitaxial growth. Both diffraction rings of PbSe, $\{200\}_{PbSe}$ and $\{220\}_{PbSe}$, show twelve equally spaced ring fragments with the fragments of $\{200\}_{PbSe}$ and $\{220\}_{PbSe}$ rotated by 45° with respect to each other. This characteristic arrangement of reflections can be consistently explained assuming an epitaxial relationship described by PbSe(001)||MoS_2(0001) (in growth direction) and PbSe(200)||MoS_2{1–100} (in plane). According to Cho et al.[46] the largest dipole moment in PbSe QDs should be along the $<001>_{PbSe}$ axis. Therefore the PbSe QDs in the PbSe-MoS_2 hybrid exhibit a dipole moment perpendicular to the MoS_2 nanoflake (see Figure S5, Supporting Information). The resulting dipole-dipole interactions between PbSe and MoS_2 are one possible explanation for the strong bonding of the PbSe QDs on the MoS_2 flakes that even withstands repeated ultrasonication.

Due to symmetry considerations there are three equivalent orientation variants of PbSe, which are related to each other by a 120° rotation around the growth axis as indicated by the three squares in Figure 2a, each interconnecting reflections of one variant. A more detailed analysis of the diffraction pattern is provided in Figure S6 (Supporting Information). The corresponding arrangement of atoms in the three orientation variants is illustrated in Figure 2b. It is interesting to note that the described orientation relationship with its three orientation variants is identical to the one observed in bulk misfit-layered compounds[47] and has also been identified for thin PbS films grown by molecular beam epitaxy onto freshly cleaved TiS_2(0001) substrates.[48] In contrast to these cases, where the {200} lattice planes of the monochalcogenide and {1–100} lattice planes of the dichalcogenide match there is a huge misfit of about 12% between the corresponding lattice planes in PbSe (d_{200}^{PbSe} = 0.3064 nm [ICSD no. 38294]) and MoS_2 ($d_{1-100}^{MoS_2}$ = 0.2737 nm [ICSD no. 84180]). This misfit is indicated in Figure 2b and revealed by the separation of the corresponding reflections in the diffraction pattern in Figure 2a. In the perpendicular in-plane direction, i.e., along $<11–20>_{MoS_2}$, there is a much better match of the two lattices as can be seen by comparing d_{400}^{PbSe} = 0.1532 nm and $d_{11-20}^{MoS_2}$ = 0.1580 nm (misfit of only 3%). This is likely to be the main reason for the observed epitaxial orientation relationship. However, a misfit of 3% is still large enough to explain the observation that the PbSe

diffraction spots in Figure 2a do not form a discrete point pattern but rather ring pattern fragments indicating that the PbSe QDs have a remaining in-plane rotational degree of freedom on the MoS_2 flakes (see illustration Figure 2c). The rotational range can be determined directly from the SAED pattern in Figure 2a and does not exceed 12° for most of the particles of each orientation variant.

The notion of epitaxial growth is further supported by HRTEM images (Figure 2d,e), in which the three orientation variants are clearly visible. Because of the small sizes of the PbSe QDs the HRTEM image contrast is dominated by the hexagonal lattice of the MoS_2 substrate. The stripe-like modulation of the HRTEM contrast in the areas covered by QDs results from interference of electrons scattered in the PbSe and in the MoS_2 (Moiré interference). In agreement with the three orientation variants and the corresponding lattice misfit (see discussion above) each PbSe QD shows modulations along one of the three $<1\text{–}100>_{MoS_2}$ lattice directions. Enlarged HRTEM images of representative QDs are depicted in Figure 2e together with their respective lattice orientation. It should be mentioned that the modulation is slightly more complex than expected from a simple Moiré analysis, which is likely due to multiple scattering, which causes various spatial frequencies along the mismatched $<1\text{–}100>_{MoS_2}$ direction. However, as can be seen from the HRTEM image in Figure 2d the three types of QDs corresponding to the different orientation variants can be clearly distinguished as indicated by the red, green, and yellow circles.

In a control experiment pre-synthesized PbSe QDs were simply mixed with MoS_2 flakes (first approach: stirring for 1 h at room temperature; second approach: heating at 170 °C for 4 h under argon atmosphere). These samples also showed PbSe QDs assembled on the MoS_2 flakes (see Figure S7, Supporting Information). However, in this case the SAED patterns (Figure 2f) of the QDs formed complete rings with constant intensity instead of points or ring fragments, thus revealing no preferential orientation of the PbSe QDs on the MoS_2 nanoflakes. Consequently, an in situ synthesis is necessary to achieve epitaxial growth of PbSe QDs on MoS_2 nanoflakes.

In summary, these results already represent strong evidence for a direct contact between the QDs and the exfoliated flakes without any linker molecules at the interface. The QDs grow epitaxially on the surface rather than attaching after formation. If ligands (i.e., oleic acid) were to cover the QD surface this would impede any direct interaction of the QDs with the MoS_2 flakes and epitaxial orientation between the QDs and the MoS_2 flakes would be impossible.

For further verification we used focused ion beam (FIB) milling to prepare thin cross-sectional TEM samples of PbSe-MoS_2 hybrid flakes. **Figure 3**a shows a bright-field (BF) TEM image of a representative multilayered MoS_2 nanoflake with a thickness of roughly 25 nm covered with PbSe QDs on both surfaces. The HRTEM image of Figure 3b clearly demonstrates that the PbSe QDs are intimately attached to the MoS_2 substrate (orange labeled region). Even though the expected layered contrast of MoS_2 with an interlayer distance of d_{0002}^{MoS2} = 0.6145 nm [ICSD no. 84180] is clearly visible in Figure 3a and 3b, the layered structure is somewhat damaged, which can be attributed to FIB milling and electron beam irradiation during TEM investigation. The original MoS_2 flakes show excellent

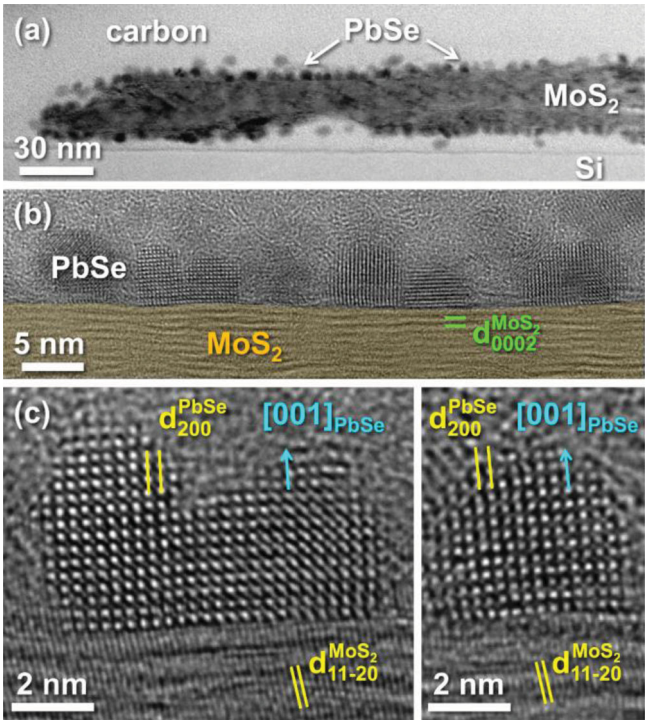

Figure 3. a) Bright-field TEM image of a cross-sectional FIB sample of the PbSe-MoS_2 hybrids on a silicon substrate, covered with a protective carbon layer. b) HRTEM image showing intimate contact between the PbSe QDs and the layered MoS_2 flake (orange labeled region) with an interlayer distance of $d_{0002}^{MoS_2}$ = 0.6145 nm. c) Two magnified HRTEM images of PbSe QDs grown on MoS_2 flakes along $[001]_{PbSe}$ direction. The preferred in-plane orientation relation deduced from plan-view SAED (Figure 2a) is reflected by the nearly parallel alignment of $\{200\}_{PbSe}$ and $\{11\text{–}20\}_{PbSe}$ lattice planes.

crystalline quality in plan-view TEM images as well as SAED and CBED patterns (Figure S2,S3, Supporting Information). The CBED measurements furthermore confirm that the thicknesses of the MoS_2 flakes are in the range of a few tens of nanometers (see example in Figure S3, Supporting Information). Thus, from an electronic point of view, the MoS_2 nanoflake can be considered a bulk semiconductor.[49]

The preferred crystallographic orientation of the PbSe QDs on the MoS_2 flakes deduced from SAED and HRTEM in plan-view geometry (Figure 2) is also visible in cross-section HRTEM images (Figure 3b,c) as most of the QDs along the investigated flake exhibit a preferred texture and HRTEM contrast. Figure 3c displays two representative QDs showing $\{200\}_{PbSe}$ lattice planes aligned with $\{11\text{–}20\}_{MoS_2}$ lattice planes of the MoS_2 substrate. In addition, the cross-sectional HRTEM images give further evidence that the QDs grow preferentially along $<001>_{PbSe}$. As expected for epitaxial orientation relation the HRTEM images in Figure 3b,c reveal an intimate contact between the two crystalline lattices without any linker group or impurity at the interface. If oleic acid were present between the PbSe QDs and the MoS_2 flake a spacer layer of about 2 nm, corresponding to the length of the oleic acid molecule, would be visible. The images clearly show that there is no gap or interlayer between PbSe and MoS_2, which further proves a direct and ligand-free growth of PbSe on MoS_2.

Oleic acid is present in these hybrids as confirmed by infrared (IR) spectroscopy (Figure S8, Supporting Information) but most likely only at the outer surface of the PbSe QDs and not at the PbSe-MoS_2 material interface. The ligand stabilization principle, i.e., ligands are only on the side of the particle that is not in direct contact with the MoS_2 nanoflake, has also been suggested by Huang et al.[50] Consequently, charge transfer from the QDs to the flakes should be fast because no insulating oleic acid is found at the interface, whereas the oleic acid protects the PbSe QDs on the outer surface against oxidation. Moreover, the formation of potential charge-recombination sites that are often created by ligand removal or exchange is prevented.

Based on the TEM images, SAED pattern, and cross-sectional HRTEM images combined with previous reports on the growth properties of pure PbSe QDs,[46,51–53] PbSe QDs on single-walled carbon nanotubes[54,55] and the chemical structure of misfit-layered compounds,[37,39] we propose the following mechanism for the epitaxial growth of PbSe QDs on the MoS_2 nanoflakes. Initially, $Pb(oleate)_2$ precursors coordinate directly onto the surface of the flakes. Coulomb attraction between the Pb^{2+} cations and the S^{2-} anions of MoS_2 may be responsible for the preferential coordination of positively charged Pb^{2+} ions on the flakes. Upon addition of the selenium precursor, the growth of PbSe QDs proceeds on the flakes and in solution. Comparing the PbSe-MoS_2 hybrids with other layered material hybrids (PbSe-WS_2 and PbSe-FLG) reveals that the density of PbSe QDs is always higher on MoS_2 and WS_2 flakes than on FLG (see Figure S9, Supporting Information). This supports the notion that the direct coordination of Pb^{2+} on the nanoflake is decisive in terms of QD nucleation and growth. The negative surface polarization of MoS_2 and WS_2 flakes caused by the presence of sulfide probably enhances the coordination of Pb^{2+} cations whereas the large π-electron system of FLG merely compensates charges. The fact that the QDs cannot be removed from the flakes by sonication and that SAED and HRTEM images show three preferential orientation variants confirm an epitaxial, linker-free and direct growth of the PbSe QDs on the MoS_2 surface. This is crucial for application in photodetectors as it is not possible to observe charge transport in films of as-synthesized PbSe QDs covered with long insulating oleic acid ligands.[56] For example, Zhang et al. reported no observable photoresponse for graphene covered with pre-synthesized, oleic acid capped PbS QDs.[33]

Next, we investigated the photoresponse of the PbSe-MoS_2 hybrid material. A lateral photodetector was fabricated on a glass substrate with interdigitated Cr/Au electrodes (distance 5 µm, total interdigitated electrode length 20 mm) by drop-casting a hexane dispersion of the PbSe-MoS_2 hybrid at 120 °C (**Figure 4**). The resulting films were investigated under ambient air conditions. A broadband halogen light source with a 1200 nm cut-off filter and an incident power of 1.6 mW was used for illumination. Overlapping multilayer MoS_2 flakes should transport charges better than just PbSe QDs, therefore we use MoS_2 as a charge transporting layer, but not as photosensitive material. The photosensitivity of the hybrid should result exclusively from the PbSe QDs. Therefore a 1200 nm cut-off filter was necessary to avoid photoresponse from pure MoS_2 that would occur at photon energies above 1.2 eV (wavelengths < 1030 nm; considering optical properties of MoS_2 bulk material). At wavelengths above 1200 nm, only PbSe QDs are excited – depending on their size – and excitons are formed. From the HRTEM images in Figure 1b we determined the size of the PbSe QDs on MoS_2 flakes to be 5.7 nm on average, which corresponds to a band gap of 0.74 eV (absorption edge 1675 nm).[57] After light absorption by the PbSe QDs, exciton dissociation is likely to occur at the PbSe-MoS_2 interface. Usually time-dependent photoluminescence quenching measurements are carried out to study exciton dissociation.[35,58] However, due to the small band gap of the PbSe QDs and thus photoluminescence only above 1600 nm (beyond InGaAs detectors) these measurements could not be performed in this case.

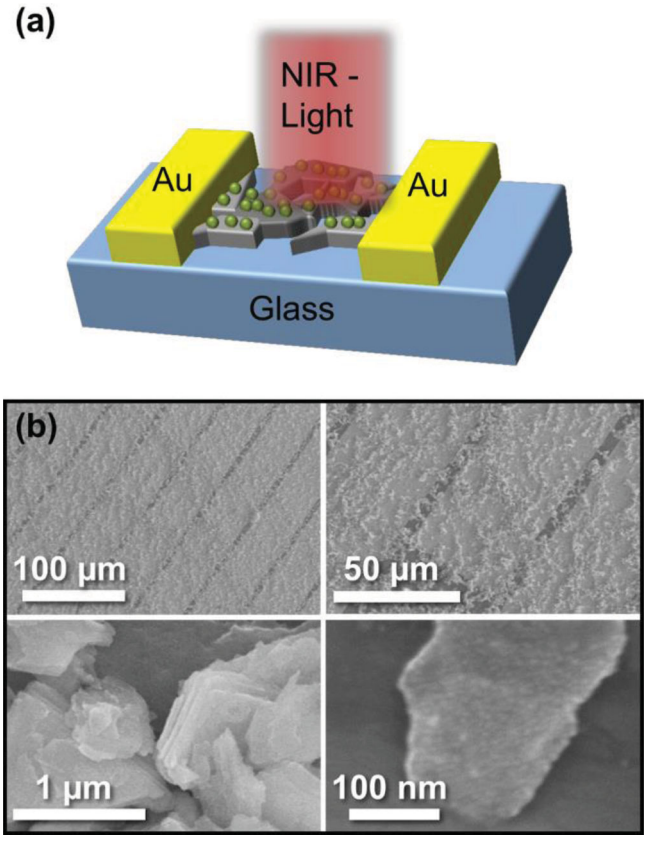

Figure 4. a) Schematic illustration of a PbSe-MoS_2 photodetector (green: PbSe QDs, gray: MoS_2 flakes). b) Scanning electron microscopy images of PbSe-MoS_2 thin films on interdigitated gold electrodes (distance 5 µm) after drop-casting a dispersion from hexane.

Figure 5 shows the photoresponse of a pristine MoS_2 film and a PbSe-MoS_2 hybrid film under applied bias as a function of illumination. Overall, a clear photo-switching behavior is observed. MoS_2 normally behaves as n-type material[6,59] and we measured a current increase rather than decrease upon illumination. Thus we infer that electrons are transferred from the PbSe QDs to the MoS_2 flakes. The charge carrier density in the MoS_2 flakes increased and the film resistance was reduced. A lower boundary of 1.9 µA/W could be estimated for the overall responsivity in the near-infrared. The photodetector was stable during operation in air and under illumination. Even after 48 cycles no considerable changes in signal strength were

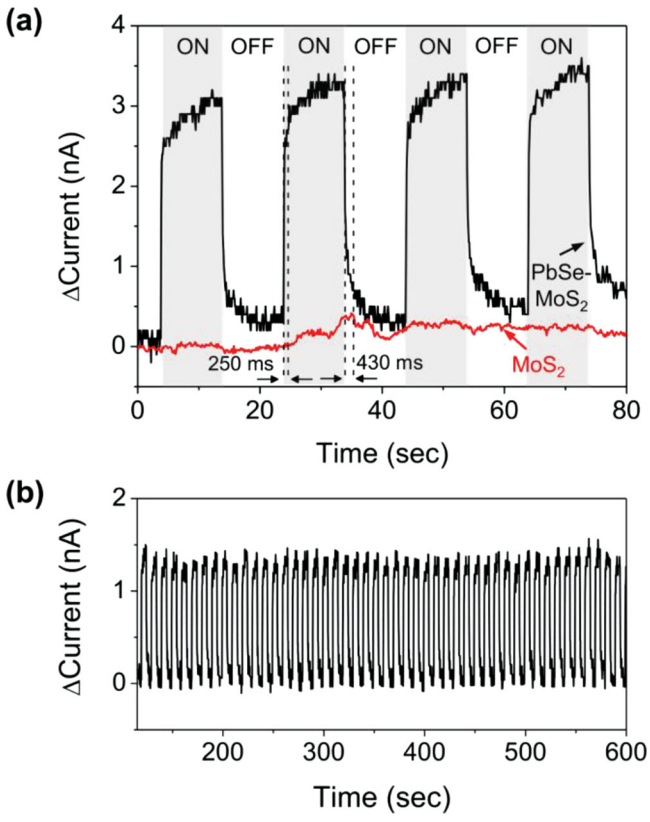

Figure 5. a) Photoresponse of a PbSe-MoS_2 (black line) and MoS_2 (red line) photodetector to incoming light ($\lambda \geq 1200$ nm). The ON-OFF switching time of the light source was 10 s, $V_{bias} = 14$ V. The dashed lines indicate the photoresponse times of this PbSe-MoS_2 photodetector. The device switches to the on-state within 250 ms and to the off-state within 430 ms. b) 48 cycles of repeated ON-OFF switching of a PbSe-MoS_2 photodetector showing excellent stability in air without degradation. The ON-OFF switching time of the light source was 5 s, $V_{bias} = 10$ V.

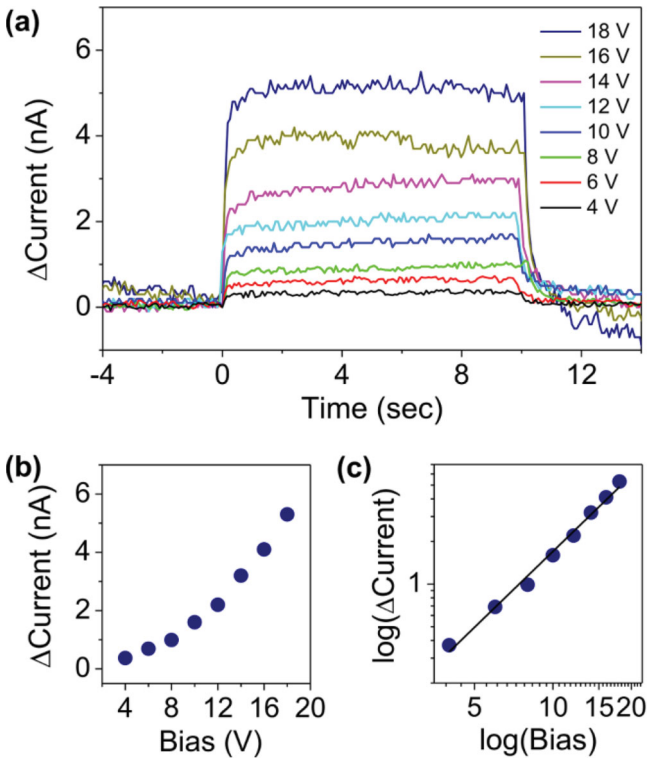

Figure 6. a) Photoresponse of a PbSe-MoS_2 photodetector at different voltages, varied from 4 V to 18 V in steps of 2 V. b) Current-bias characteristics and the corresponding c) log(ΔCurrent)–log(Bias) plot with linear fit (black line) indicates a $V_{bias}{}^n$ relation of signal with bias with $n \approx 1.5$ for voltages > 4 V.

detected (Figure 5b). Note, that the dark current of the photodetector initially increased over time while a constant bias was applied before saturating at a relatively high value (hundreds of nA, see Figure S10, Supporting Information). This behavior was not observed for the pure MoS_2 nanosheets, for which dark currents were also somewhat lower. Charge transfer is known to take place from the MX (i.e., PbSe) part to the TX_2 (i.e., MoS_2) layer in misfit-layered compounds.[40,41] It is thus conceivable that the MoS_2 was slightly doped by the attached PbSe QDs even before illumination. After stabilization of the dark current however, the photocurrent increase and decrease characteristics were symmetric. Both responses consist of two components: An initial, fast rising component (from about 0% to 75% of maximum signal) and a slower component (from about 75% to 100%). The fast component is used to determine the photoresponse time featuring a switch-on time of 160–250 ms and a switch-off time of 430–600 ms (Figure 5a). The slow component is probably related to traps originating from surface states or defects of the QDs.[28,60] The fast component is likely to depend on the mobility of the charge carriers in the film. Konstantatos et al.[28] reported a PbS-graphene photodetector with response times as short as 10 ms. Clearly, using MoS_2 nanoflake thin films rather than graphene results in much slower switching due to lower carrier mobilities and the need for hopping between flakes. A pure MoS_2 photodetector based on a large monolayer flake was shown to exhibit response times of 50 ms.[8]

We investigated the dependence of the photoresponse on the applied bias (V_{bias}) from 4 V to 18 V in steps of 2 V. **Figure 6** shows that the photocurrent increases with bias. We can exclude a single exponential dependence. A double logarithmic plot, as presented in Figure 6c, indicates a $V_{bias}{}^n$ relation of the photocurrent with bias (with $n \approx 1.5$). Increasing the applied bias may enhance exciton dissociation and suppresses charge recombination. Shorter electrode distances as well as a more uniform coverage should improve performance further.

Most importantly, these devices work in ambient air and show no degradation even after weeks of storage in air and under illumination. We attribute this remarkable stability to the fact that the PbSe QDs are still capped with long oleic acid ligands on their outer surface, while charge separation occurs directly at the interface with the MoS_2 nanoflake, where no linker is present due to the epitaxial growth of PbSe QDs. The good surface passivation of PbSe QDs with oleic acid ligands prevents the formation of quenching sites and protects them against oxidation. Usually the ligands have to be removed or exchanged in order to facilitate charge separation and transport in QD-photodetectors, which makes them sensitive to air.[28,34]

We also fabricated control devices by drop-casting as-synthesized PbSe QDs and pre-synthesized PbSe QDs mixed with

exfoliated MoS_2 (prepared by stirring at room temperature for 1 h). The PbSe-only device behaved completely insulating and showed no photoresponse at all. In the case of the PbSe QDs mixed with MoS_2 we measured a photoresponse, which was substantially weaker compared to the photoresponse of the in situ synthesized hybrids. As already mentioned above, simple mixing of pre-synthesized PbSe QDs with MoS_2 nanoflakes resulted in hybrids without any preferred orientation of the QDs (see Figure S7, Supporting Information). Therefore, the inferior photoresponse is likely to be a result of an indirect contact between the two materials, possibly still separated by the capping ligand oleic acid.

Since our photoactive PbSe-MoS_2 hybrid material was dispersed in hexane and no high-temperature fabrication processes were necessary, we were able to fabricate flexible photodetectors. To prepare these devices we drop-cast the PbSe-MoS_2 hybrid material on a PET substrate with interdigitated Cr/Au electrodes (distance 5 µm, total electrode length 20 mm) at 50 °C (**Figure 7**). These flexible devices were bent perpendicular to the electrodes and measured under the same conditions as the devices on glass, with an applied bias of 10 V. When bending the device inward (active layer under compressive stress) we observed an increase of photocurrent (Figure 7a), whereas during outward bending (active layer under tensile stress) the photocurrent decreased (Figure 7b). Both inward and outward bending were reversible and the photocurrent for the flat position after bending was almost unchanged. The devices showed clear and stable photoresponse up to the smallest measureable bending radii of r = 3.8 mm for inward bending and r = 2.9 mm for outward bending. Figure 7c shows the device performance in flat position after a number of bending cycles. Even after bending the device 400 times (first 200 times outward bending, r = 4.4 mm; then 200 times inward bending, r = 4.3 mm) we found only a small decrease in photocurrent and still a clear and stable photoresponse thus demonstrating the excellent mechanical stability of these PbSe-MoS_2 photodetectors. Our experiments clearly demonstrate that the PbSe-MoS_2 hybrid material can withstand small bending radii and repeated bending, which is important for possible applications in flexible and lightweight sensors.

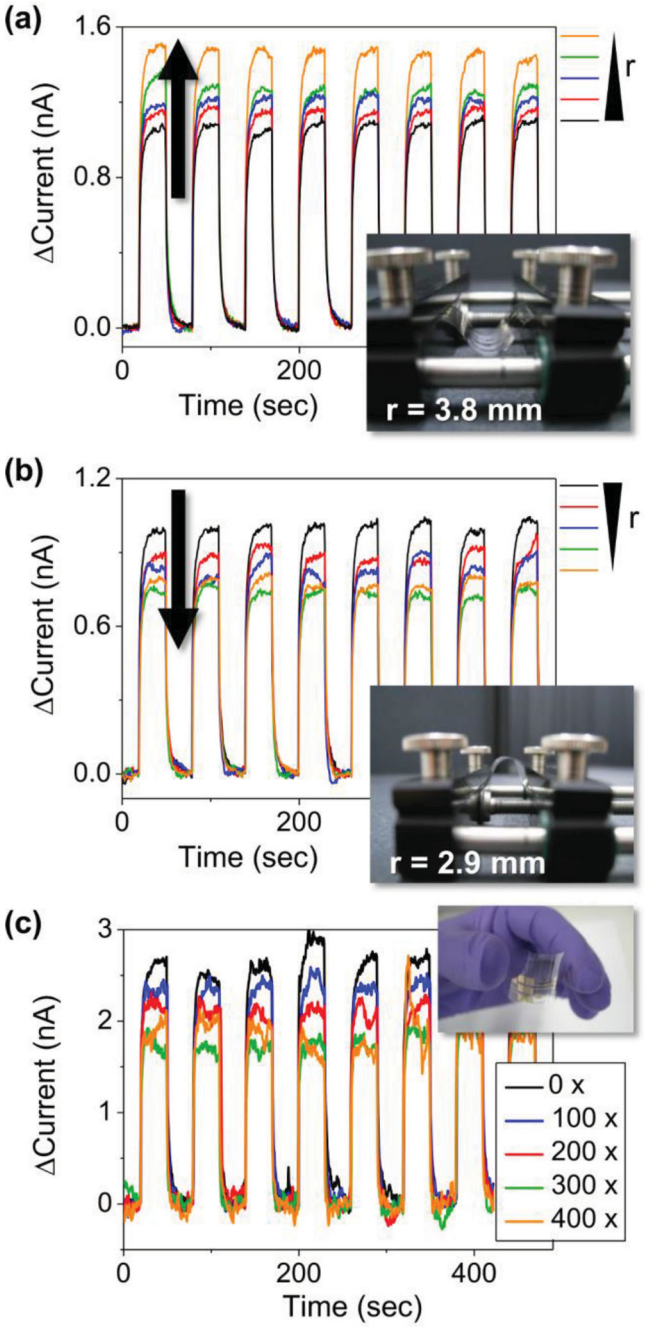

Figure 7. Photoresponse of a PbSe-MoS_2 photodetector fabricated on a flexible PET substrate. a) Bending the device inward up to a bending radius of 3.8 mm results in an increasing photocurrent whereas b) bending the device outward (maximum measureable bending radius 2.9 mm) leads to a photocurrent decrease. c) Excellent stability of the device upon repeated bending of 400 times (200 times outward bending, r = 4.4 mm; then 200 times inward bending, r = 4.3 mm). The ON-OFF switching time of the light source was 30 s, V_{bias} = 10 V.

3. Conclusions

In summary, we have developed a facile one-pot synthesis of PbSe-MoS_2 hybrids. This simple wet-chemical synthesis provides an effective way to grow PbSe QDs without any linker groups on many kinds of layered materials such as MoS_2, WS_2, and FLG. The observed epitaxial growth of the PbSe QDs on the MoS_2 nanoflakes with three equivalent orientation variants (120° relative orientation to each other) as well as cross-sectional HRTEM images verify a direct contact between the two materials. Oleic acid ligands on the outer surface of the PbSe QDs ensure protection and air-stability. No laborious linker-exchange steps are necessary and the hybrid materials are stable in ambient air. Solution-processed photodetectors based on PbSe QDs on MoS_2 flakes exhibit clear and stable photoconductivity when illuminated with near-IR light (λ > 1200 nm). Flexible devices fabricated on PET substrates show excellent stability upon repeated bending at small bending radii. Due to the air-stability and solution-processability of the PbSe-MoS_2 hybrids, and the tunability of the PbSe QD size by growth time, these hybrid materials are promising for low-cost and flexible near-IR photodetectors.

4. Experimental Section

Chemicals: All chemicals were obtained from commercial sources. MoS_2 powder (particle size < 2 μm), WS_2 powder (particle size < 2 μm), graphite flakes (particle size +100 mesh; ≥75% min)), lead oxide, tri-*n*-octylphosphine, selenium powder, diphenyl ether (≥99%), 1-octadecene (technical grade 90%), oleic acid (≥99.0%), hexane, methanol, and acetone were purchased from Sigma Aldrich, ethanol was purchased from Carl Roth GmbH.

MoS_2, WS_2, and Graphite Exfoliation: MoS_2 and WS_2 were used as received. The graphite powder was sieved through a 0.5 mm mesh to remove large particles. MoS_2, WS_2, or graphite (20 mg) were dispersed in diphenyl ether (10 mL) by sonication in an ultrasonic bath (Branson 2510) for 1 h followed by vigorous sonication using a tip sonicator (Sonics Vibra Cell) running at 25% of maximum power for 10 min. After centrifugation at 500 rpm for 45 min (Beckman Coulter Avanti J26XP centrifuge) the dispersion was allowed to settle for 2 h. The supernatant contained exfoliated MoS_2 flakes, exfoliated WS_2 flakes, or few-layered graphene (FLG). Subsequently, 5 mL of the respective supernatant were used for synthesis.

Synthesis of Hybrid Materials: In situ synthesis of PbSe-MoS_2 hybrids was performed in argon atmosphere using a standard air-free Schlenk-line technique and hot-injection. For a typical synthesis a stock solution of $Pb(oleate)_2$ was prepared by dissolving PbO (225 mg, 1 mmol) and oleic acid (1 ml, 3.14 mmol) in 1-octadecene (7.5 mL). The reaction mixture was dried in vacuum at 100 °C for 1 h. It was then heated to 120 °C under moderate argon flow. 5 mL of the respective nanoflake dispersion (MoS_2, or WS_2, FLG) was injected into the $Pb(oleate)_2$ stock solution and the mixture was again dried at 100 °C for about 30–60 min. It was then heated to 170 °C under moderate argon flow and tri-*n*-octylphosphine selenium (TOPSe) (1.8 mL, 2 mmol; 438.3 mg Se/5 mL TOP) solution was rapidly injected. The reaction mixture was kept at 150 °C for 5 min and then quenched with a cold water bath. The PbSe-MoS_2 hybrids were washed four times with hexane, hexane/ethanol/methanol, hexane, and hexane by centrifugation at 10 000 g for 15 min to remove all contaminants and free PbSe QDs. The PbSe-MoS_2 hybrids were redispersed in hexane for further measurements. PbSe QDs were synthesized as follows: A stock solution of $Pb(oleate)_2$ was prepared by dissolving PbO (225 mg, 1 mmol) and oleic acid (1 mL, 3.14 mmol) in 1-octadecene (7.5 mL). The reaction mixture was dried in vacuum at 100 °C for 1 h. It was then heated to 170 °C under moderate argon flow and TOPSe (1.8 mL, 2 mmol; 438.3 mg Se/5 mL TOP) solution was rapidly injected. The reaction mixture was kept at 150 °C for 5 min and then quenched with a cold water bath. The PbSe QDs were washed three times with hexane/acetone, hexane/ethanol/acetone, and hexane by centrifugation at 6000 rpm for 5 min. The same procedure was used for PbSe-FLG and PbSe-WS_2 hybrids.

Characterization of Hybrid Materials: All spectra and images were obtained at room temperature. Raman spectra were acquired with a Renishaw inVia Reflex Confocal Raman Microscope with an excitation laser wavelength of 532 nm (MoS_2, FLG) and 633 nm (WS_2). High-resolution (HR) and bright-field (BF) transmission electron microscopy (TEM) images, selected-area electron diffraction (SAED) patterns, and energy-dispersive X-ray spectroscopy (EDX) spectra were recorded with an aberration-corrected Titan^3 transmission electron microscope operated at 80 kV acceleration voltage in order to minimize electron-beam induced damage. SAED pattern to confirm a preferred orientation of PbSe QDs on MoS_2 were obtained with a Philips CM 300 UT operated at 300 kV. CBED pattern to determine the thickness of the MoS_2 flakes were performed using a Philips CM 30 operated at 300 kV. Samples were prepared by drop-casting a dispersion of hybrid materials onto a 200 mesh lacey carbon copper grid. Scanning electron microscope (SEM) images were taken with a Hitachi FE-SEM S4800 microscope. Cross-sectional samples of the PbSe-MoS_2 hybrids were prepared using a FEI Helios NanoLab 660 focused ion beam (FIB). For the preparation the hybrid dispersion was drop-cast on a silicon wafer substrate and covered with a carbon layer in the FIB to protect the sensitive material from the ion beam. A thin lamella was cut using the Ga^+ ion beam of the FIB. For final polishing the acceleration voltage of the Ga^+ beam was reduced from 30 kV down to 2 kV. The lamella was then transferred to an Omniprobe TEM grid using the lift-out technique.

Fabrication and Characterization of PbSe-MoS_2 Photodetectors: Interdigitated electrodes (2 nm Cr, 30 nm Au, electrode distance 5 μm; overall electrode length 20 mm) were defined photolithographically using a standard double-layer photoresist (LOR5B/S1813), electron-beam evaporation and lift-off process on glass or polyethylene terephthalate (PET) substrates. Before hybrid material deposition the substrates were cleaned with acetone and isopropanol in an ultrasonic bath and subsequently rinsed with deionized water. The PbSe-MoS_2 hybrid dispersion was drop-cast from hexane on the pre-patterned interdigitated electrodes at a temperature of 120 °C for glass and 50 °C for PET. Photocurrent measurements were carried out at room temperature in air with an Agilent 4155C semiconductor parameter analyzer and a broadband halogen light source (HL 2000 from Ocean Optics) with a 1200 nm cut-off filter.

Supporting Information

Supporting Information is available from the Wiley Online Library or from the author.

Acknowledgements

J.S. and B.W. contributed equally to this work. This research was financially supported by the Excellence Cluster "Engineering of Advanced Materials" (DFG EXC 315) and the Alfried Krupp von Bohlen und Halbach-Stiftung. J.S. gratefully acknowledges the Erlangen Graduate School in Advanced Optical Technologies (SAOT) within the framework of the German Excellence Initiative (DFG GSC 80) and B.W. acknowledges the Research Training Group "Disperse Systems for Electronic Applications" (GRK 1161). The authors thank C. Dieker (CENEM) for FIB sample preparation and A. Friedrich for help with SEM measurements.

Received: January 29, 2014
Revised: April 26, 2014
Published online: July 14, 2014

[1] A. D. Yoffe, *Annu. Rev. Mater. Sci.* **1973**, *3*, 147.
[2] K. F. Mak, C. Lee, J. Hone, J. Shan, T. F. Heinz, *Phys. Rev. Lett.* **2010**, *105*, 136805.
[3] M. Xu, T. Liang, M. Shi, H. Chen, *Chem. Rev.* **2013**, *113*, 3766.
[4] X. Song, J. Hu, H. Zeng, *J. Mater. Chem. C* **2013**, *1*, 2952.
[5] M. Chhowalla, H. S. Shin, G. Eda, L.-J. Li, K. P. Loh, H. Zhang, *Nat. Chem.* **2013**, *5*, 263.
[6] B. Radisavljevic, A. Radenovic, J. Brivio, V. Giacometti, A. Kis, *Nat. Nanotechnol.* **2011**, *6*, 147.
[7] Q. H. Wang, K. Kalantar-Zadeh, A. Kis, J. N. Coleman, M. S. Strano, *Nat. Nanotechnol.* **2012**, *7*, 699.
[8] Z. Yin, H. Li, H. Li, L. Jiang, Y. Shi, Y. Sun, G. Lu, Q. Zhang, X. Chen, H. Zhang, *ACS Nano* **2012**, *6*, 74.
[9] S. Kim, A. Konar, W.-S. Hwang, J. H. Lee, J. Lee, J. Yang, C. Jung, H. Kim, J.-B. Yoo, J.-Y. Choi, Y. W. Jin, S. Y. Lee, D. Jena, W. Choi, K. Kim, *Nat. Commun.* **2012**, *3*, 1011.
[10] H. S. Lee, S.-W. Min, Y.-G. Chang, M. K. Park, T. Nam, H. Kim, J. H. Kim, S. Ryu, S. Im, *Nano Lett.* **2012**, *12*, 3695.
[11] J. N. Coleman, M. Lotya, A. O'Neill, S. D. Bergin, P. J. King, U. Khan, K. Young, A. Gaucher, S. De, R. J. Smith, I. V. Shvets, S. K. Arora, G. Stanton, H.-Y. Kim, K. Lee, G. T. Kim, G. S. Duesberg, T. Hallam,

J. J. Boland, J. J. Wang, J. F. Donegan, J. C. Grunlan, G. Moriarty, A. Shmeliov, R. J. Nicholls, J. M. Perkins, E. M. Grieveson, K. Theuwissen, D. W. McComb, P. D. Nellist, V. Nicolosi, *Science* **2011**, *331*, 568.
[12] C. Lee, H. Yan, L. E. Brus, T. F. Heinz, J. Hone, S. Ryu, *ACS Nano* **2010**, *4*, 2695.
[13] W. Choi, M. Y. Cho, A. Konar, J. H. Lee, G.-B. Cha, S. C. Hong, S. Kim, J. Kim, D. Jena, J. Joo, S. Kim, *Adv. Mater.* **2012**, *24*, 5832.
[14] W. Zhang, J.-K. Huang, C.-H. Chen, Y.-H. Chang, Y.-J. Cheng, L.-J. Li, *Adv. Mater.* **2013**, *25*, 3456.
[15] Y. Wang, N. Herron, *Chem. Phys. Lett.* **1992**, *200*, 71.
[16] N. C. Greenham, X. Peng, A. P. Alivisatos, *Phys. Rev. B* **1996**, *54*, 17628.
[17] H. Mattoussi, L. H. Radzilowski, B. O. Dabbousi, E. L. Thomas, M. G. Bawendi, M. F. Rubner, *J. Appl. Phys.* **1998**, *83*, 7965.
[18] D. S. Ginger, N. C. Greenham, *J. Appl. Phys.* **2000**, *87*, 1361.
[19] S. A. McDonald, G. Konstantatos, S. Zhang, P. W. Cyr, E. J. D. Klem, L. Levina, E. H. Sargent, *Nat. Mater.* **2005**, *4*, 138.
[20] G. Konstantatos, I. Howard, A. Fischer, S. Hoogland, J. Clifford, E. Klem, L. Levina, E. H. Sargent, *Nature* **2006**, *442*, 180.
[21] M. Böberl, M. V. Kovalenko, S. Gamerith, E. J. W. List, W. Heiss, *Adv. Mater.* **2007**, *19*, 3574.
[22] J. P. Clifford, G. Konstantatos, K. W. Johnston, S. Hoogland, L. Levina, E. H. Sargent, *Nat. Nanotechnol.* **2009**, *4*, 40.
[23] G. Konstantatos, E. H. Sargent, *Nat. Nanotechnol.* **2010**, *5*, 391.
[24] Z. Ning, Y. Ren, S. Hoogland, O. Voznyy, L. Levina, P. Stadler, X. Lan, D. Zhitomirsky, E. H. Sargent, *Adv. Mater.* **2012**, *24*, 6295.
[25] D. Wang, J. K. Baral, H. Zhao, B. A. Gonfa, V.-V. Truong, M. A. El Khakani, R. Izquierdo, D. Ma, *Adv. Funct. Mater.* **2011**, *21*, 4010.
[26] V. Georgakilas, D. Gournis, V. Tzitzios, L. Pasquato, D. M. Guldi, M. Prato, *J. Mater. Chem.* **2007**, *17*, 2679.
[27] X. Peng, J. Chen, J. A. Misewich, S. S. Wong, *Chem. Soc. Rev.* **2009**, *38*, 1076.
[28] G. Konstantatos, M. Badioli, L. Gaudreau, J. Osmond, M. Bernechea, F. P. G. de Arquer, F. Gatti, F. H. L. Koppens, *Nat. Nanotechnol.* **2012**, *7*, 363.
[29] Y. Lin, K. Zhang, W. Chen, Y. Liu, Z. Geng, J. Zeng, N. Pan, L. Yan, X. Wang, J. G. Hou, *ACS Nano* **2010**, *4*, 3033.
[30] A. Cao, Z. Liu, S. Chu, M. Wu, Z. Ye, Z. Cai, Y. Chang, S. Wang, Q. Gong, Y. Liu, *Adv. Mater.* **2010**, *22*, 103.
[31] K. Yu, G. Lu, S. Mao, K. Chen, H. Kim, Z. Wen, J. Chen, *ACS Appl. Mater. Interfaces* **2011**, *3*, 2703.
[32] K. K. Manga, J. Wang, M. Lin, J. Zhang, M. Nesladek, V. Nalla, W. Ji, K. P. Loh, *Adv. Mater.* **2012**, *24*, 1697.
[33] D. Zhang, L. Gan, Y. Cao, Q. Wang, L. Qi, X. Guo, *Adv. Mater.* **2012**, *24*, 2715.
[34] Z. Sun, Z. Liu, J. Li, G.-a. Tai, S.-P. Lau, F. Yan, *Adv. Mater.* **2012**, *24*, 5878.
[35] S. Guo, D. Bao, S. Upadhyayula, W. Wang, A. B. Guvenc, J. R. Kyle, H. Hosseinibay, K. N. Bozhilov, V. I. Vullev, C. S. Ozkan, M. Ozkan, *Adv. Funct. Mater.* **2013**, *23*, 5199.
[36] E. Spiecker, M. Garbrecht, W. Jäger, K. Tillmann, *J. Microsc.* **2010**, *237*, 341.
[37] M. M. Smeller, C. L. Heideman, Q. Lin, M. Beekman, M. D. Anderson, P. Zschack, I. M. Anderson, D. C. Johnson, *Z. Anorg. Allg. Chem.* **2012**, *638*, 2632.
[38] G. A. Wiegers, *Prog. Solid State Chem.* **1996**, *24*, 1.
[39] J. Rouxel, A. Meerschaut, G. A. Wiegers, *J. Alloys Compd.* **1995**, *229*, 144.
[40] J. Brandt, L. Kipp, M. Skibowski, E. E. Krasovskii, W. Schattke, E. Spiecker, C. Dieker, W. Jäger, *Surf. Sci.* **2003**, *532–535*, 705.
[41] E. Kabliman, P. Blaha, K. Schwarz, *Phys. Rev. B* **2010**, *82*, 125308.
[42] V. Komanicky, H. Iddir, K.-C. Chang, A. Menzel, G. Karapetrov, D. Hennessy, P. Zapol, H. You, *J. Am. Chem. Soc.* **2009**, *131*, 5732.
[43] J. A. Enterkin, K. R. Poeppelmeier, L. D. Marks, *Nano Lett.* **2011**, *11*, 993.
[44] T. Sekitani, T. Yokota, U. Zschieschang, H. Klauk, S. Bauer, K. Takeuchi, M. Takamiya, T. Sakurai, T. Someya, *Science* **2009**, *326*, 1516.
[45] T. Sekitani, U. Zschieschang, H. Klauk, T. Someya, *Nat. Mater.* **2010**, *9*, 1015.
[46] K.-S. Cho, D. V. Talapin, W. Gaschler, C. B. Murray, *J. Am. Chem. Soc.* **2005**, *127*, 7140.
[47] S. Kuypers, J. Van Landuyt, S. Amelinckx, *J. Solid State Chem.* **1990**, *86*, 212.
[48] E. Spiecker, *Microsc. Microanal.* **2003**, *9*, 300.
[49] T. Li, G. Galli, *J. Phys. Chem. C* **2007**, *111*, 16192.
[50] X. Huang, Z. Zeng, S. Bao, M. Wang, X. Qi, Z. Fan, H. Zhang, *Nat. Commun.* **2013**, *4*, 1444.
[51] A. J. Houtepen, R. Koole, D. Vanmaekelbergh, J. Meeldijk, S. G. Hickey, *J. Am. Chem. Soc.* **2006**, *128*, 6792.
[52] Y.-w. Jun, J.-s. Choi, J. Cheon, *Angew. Chem., Int. Ed.* **2006**, *45*, 3414.
[53] C. Fang, M. A. van Huis, D. Vanmaekelbergh, H. W. Zandbergen, *ACS Nano* **2010**, *4*, 211.
[54] X. Chen, X. Huang, L. Kong, Z. Guo, X. Fu, M. Li, J. Liu, *J. Mater. Chem.* **2010**, *20*, 352.
[55] J. Schornbaum, B. Winter, S. P. Schießl, B. Butz, E. Spiecker, J. Zaumseil, *Chem. Mater.* **2013**, *25*, 2663.
[56] D. V. Talapin, C. B. Murray, *Science* **2005**, *310*, 86.
[57] I. Moreels, K. Lambert, D. De Muynck, F. Vanhaecke, D. Poelman, J. C. Martins, G. Allan, Z. Hens, *Chem. Mater.* **2007**, *19*, 6101.
[58] I. V. Lightcap, P. V. Kamat, *J. Am. Chem. Soc.* **2012**, *134*, 7109.
[59] H. Nam, S. Wi, H. Rokni, M. Chen, G. Priessnitz, W. Lu, X. Liang, *ACS Nano* **2013**, *7*, 5870.
[60] G. Konstantatos, L. Levina, J. Tang, E. H. Sargent, *Nano Lett.* **2008**, *8*, 4002.